Ore Geology Reviews 89 (2017) 132–142

Contents lists available at ScienceDirect

Ore Geology Reviews

journal homepage: www.elsevier.com/locate/oregeo

Chromite typology and composition characterized through multispectral specular reflectance

Alfredo López-Benito [a,*], Fernando Gervilla [b], Juan C. Catalina [c], Ricardo Castroviejo [c]

[a] Universidad Politécnica de Madrid, Center for Computational Simulation, Department of Geological and Mining Engineering, Ríos Rosas, 21, 28003 Madrid Spain
[b] University of Granada, Department of Mineralogy and Petrology, Av. Fuentenueva s/n, 18002 Granada Spain
[c] Universidad Politécnica de Madrid, Department of Geological and Mining Engineering, Ríos Rosas, 21, 28003 Madrid Spain

ARTICLE INFO

Article history:
Received 22 February 2017
Received in revised form 25 May 2017
Accepted 8 June 2017
Available online 13 June 2017

Keywords:
Chromite
Typological characterization
Multispectral reflectance
VNIR
CAMEVA System
Image analysis

ABSTRACT

Determination of multispectral specular reflectance is an important tool for ore identification in reflected light microscopy, and may be used for automated characterization of ores. However, reflectance values can be affected by compositional variations in a way that is seldom understood. The aim of the present work is to investigate this problem in chromite, an ore whose composition may show typically large natural variations as member of the spinel family, and whose relatively high reflectance variations are apparently unpredictable. For this research, eighteen samples of chromian spinel covering a large range of compositions in the base of the Hagerthy prism were selected for microprobe analysis and reflectance measure on polished sections. The samples belong to a variety of deposits and types (ultramafic massif, ophiolitic, and metamorphosed types: Ojén and Ronda Massifs, Spain; Mayarí, Moa-Baracoa, Camagüey and Sagua de Tánamo, Cuba; Golyamo Kemenyane, Avren and Yakovitsa, Bulgaria). The specular reflectances are characterized as multispectral values, measured at thirteen intervals (50 nm each) in the VNIR region (Visible and Near-Infrared: 400–1000 nm), using the automated CAMEVA System.

The relationship between compositional and reflectance values is studied by multivariate analysis and subsequently tested on independent samples. For this purpose, the samples have been grouped in two sets: a larger population of fifteen samples constitutes the initial data set for mathematical processing, while a selection of three samples of widely differing compositions is used to test the resulting functions, so as to gain a critical appraisal of their validity.

The results obtained show that the specular reflectance of chromite depends on composition and can be used to estimate compositional parameters, as #Cr = Cr/(Cr + Al) or #Mg = Mg/(Mg + Fe^{2+}), but this relationship is complex and does not allow simple direct determinations, due to the multiplicity of possible changes and coupled substitutions (e.g. Al–Cr–Fe^{3+}, or Mg-Fe^{2+}, Ni, Zn, Ti ...) in the chromian spinel family. On the other hand, the relationship of chromite composition with deposit type is also detectable through the reflectance values, but with a higher uncertainty. Reflectance increases with increasing Cr and Fe^{3+} contents in all cases, but the relationship of reflectance with Mg seems to be specific of the deposit type: while reflectance increases with increasing #Mg in the Ojén chromites, it shows the opposite behaviour in podiform chromites. Although these results should be regarded as preliminary until further studies on larger sample populations can be achieved, they are suggestive of possible practical applications for exploration, e. g. to approach Cr-spinel compositions or chromite deposit typology, early in an exploration campaign, by inexpensive reflected light determination of specular reflectance in a few samples.

1. Introduction

Ore microscopy found its application as a tool to support ore processing as soon as the reflected light microscopy of anisotropic materials was understood (Freund, 1966). The need for objective measures to complement subjective observations arose also very soon, and was addressed in various ways. Along the 20th century, ore identification benefitted from precise quantitative specular reflectance, R,[1] and VHN measures and point counter devices were

[1] Specular reflectance is the ratio of the intensity reflected normally by a polished surface and the incident intensity (Criddle, 1998); this author provides a clear introduction to the methodological requirements also discuses in Criddle and Stanley (1993). Usually, it is expressed as a percentage of the incident intensity. Since we have use dry objectives for all measures, only values of reflectance in air will be referred here.

* Corresponding author.
E-mail address: alfredo.lopez@upm.es (A. López-Benito).

http://dx.doi.org/10.1016/j.oregeorev.2017.06.010
0169-1368/

designed to quantify process mineralogy information (modal analysis, grain size, liberation analysis, etc.). The ever increasing demand for this type of information by modern industry required a further step: automation, either by optical or by SEM-based systems. The latter are powerful, but their high price precludes extensive use. However, recent improvements in optics, electronics and computer science allow designing, at a much lower price, competitive automated systems based on optical microscopy, as the CAMEVA System used for this work (Pirard et al., 2008; Catalina and Castroviejo, 2016).

The CAMEVA System measures multispectral reflectance values in the VNIR realm (Visible and Near-Infra-Red) and compares them with the spectral information of a specific database (Castroviejo et al., 2014) to identify each mineral species. The method, which has been successfully applied to a number of industrial problems, is based on the assumption that ores can be identified by their VNIR spectra, an assumption that has been tested and validated for common ores (Castroviejo et al., 2009; Brea et al., 2010). This might be done with a spectrometer coupled to a microscope and to a computer with digitalized QDF3 files in the visible region (Criddle and Stanley, 1993), as described by Bernhardt (1987), but then the automation is limited to the ore identification in the single point measured (a μm-size spot) and no other data (e.g. modal analyses, grain size) can be compiled, so no automated image analysis is possible. The CAMEVA System is designed to work with digital images, on which all the measures are done on a pixel to pixel basis, instead of measuring just blind spots. This way, once the images of polished ore sections have been acquired, all the information is ready for image analysis (Castroviejo et al., 2010) and can be mathematically processed for any purpose, e. g. ore identification, modal content, grain-size, textural analysis, etc.

While the systematic application of the method to different kinds of ores provides a sound validation of the system (Castroviejo et al., 2009; Brea et al., 2010), some ores provide particular challenges for research, e.g. the relationship of reflectance values and composition in isomorphic phases or in mineral groups with large compositional variations. Chromite is a typical example, as a member of the spinel family whose industrial use (and value) depends largely on its composition. The purpose of this work is to ascertain the relationship of compositional and reflectance values in different types of chromites and to test the possibility to determine chromite compositions optically. For this purpose, the VNIR spectra of selected ores with known typologies and compositions are compared, so that the relationships between specular reflectance values and composition can be analysed. Published works on the application of reflectance measurements to the characterization of Cr-spinels (Eales, 1980; López-Benito et al., 2015) or on the spectral reflectance-compositional properties of spinels and chromites applied to remote sensing (Clark et al., 1990; Okada and Iwashita, 1992; Cloutis et al., 2004; Cloutis et al., 2010; Carli and Sgavetti, 2011; Williams et al., 2016) support this aim.

2. Materials and methods

2.1. Ore types and compositions

Two main world-wide types of chromite ore deposits are presently in production: those related to layered igneous intrusions (stratiform ores) and those located in the mantle section of ophiolite sequences (podiform ores). Other types of chromite occurrences, as well as metamorphic modifications of the main types (e.g. in ophiolites), are also known. The ores chosen for this work were selected from 18 samples described by Gervilla and Leblanc (1990), Proenza et al. (1999), Henares et al. (2010), González-Jiménez et al. (2011), Gervilla et al. (2012) and Colas et al. (2014). These samples include podiform ores from eastern and central Cuban ophiolites (Proenza et al., 1999; Henares et al., 2010; González-Jiménez et al., 2011), chromite ores from the Ojén ultramafic massifs overlapping the composition of stratiform chromite ores in terms of their #Cr (#Cr = Cr/(Cr + Al)) and #Mg (#Mg = Mg/(Mg + Fe^{2+})) (Gervilla and Leblanc, 1990), samples of Cr-poor chromian spinel from undescribed, nearly massive layers of "spinelites" from the Ronda ultramafic massif and some metamorphosed podiform ores from the Golyamo Kamenyane, Yakovitsa and Avren serpentinite massifs in Bulgaria (Gervilla et al., 2012; Colas et al., 2014) (see Fig. 1).

Selection criteria were fixed to cover an appropriate compositional range for chromites. Since the role played by Fe^{3+} in the reflectance of stratifom chromites was already shown by Eales (1980), the samples used in this study were selected to cover a wide compositional area in the Fe^{3+}-free (or Fe^{3+}-poor) base of the spinel prism (Fig. 1), thus allowing to check the role played by other single major cations or combinations of cations in the reflectance of chromite. The scarcity of natural samples with Fe^{3+}-free (or even Fe^{3+}-poor) composition close to the $FeCr_2O_4$ and $MgCr_2O_4$ corners of the spinel prism hindered obtaining reflectance measures of these two Cr-rich regions. The only sample with Cr/(Cr + Al) > 0.8 (GK3A-1) contains significant amounts of Fe_2O_3 (9,36 wt%). Although Fe_2O_3 can modify the reflectance of chromian spinel, increasing it substantially, the results obtained by Eales (see Eales (1980), Fig. 7) suggest that Fe_2O_3 contents below 10% (wt.) should not significantly alter the results expected in this study, i.e. the reflectance values for Fe_2O_3 contents below 10% (wt.) remain in the typical chromite range (12–16%), clearly below magnetite values (ca. 20%).

From a typological point of view, the samples selected belong to three groups or deposit types: Serranía de Ronda ultramafic massifs (chromites from the Ojén massif and spinels from the Ronda massif), podiform (ophiolitic) chromitites, and metamorphosed ophiolites (Table 1). Their compositions are projected onto the base of the Haggerty's spinel prism (#Fe^{2+}–#Cr plane) (Haggerty, 1976) and compared to published data of other world deposits in Fig. 1, showing how the samples used in this study follow the two main trends stated by Barnes and Roeder (2001): Cr–Al trend (ophiolitic massifs) and Fe–Ti trend (Ojén massif). This figure shows the location of samples from Stillwater (Lenaz et al., 2012), Bushveld (Naldrett et al., 2009), Zimbabwe (Zhou and Kerrich, 1992), Mayarí (González-Jiménez et al., 2011), Golyamo Kamenyane (Gervilla et al., 2012), as well as typical published compositions from chromitites hosted by subcontinental lithospheric mantle rocks outcropping as the Serranía de Ronda ultramafic massifs in the Málaga province in southern Spain (Gervilla and Leblanc, 1990). However, as evidenced in Fig. 1, this province includes a variety of compositions, of which two types are analysed in this work: the chromites from the Ojén massif plot in a region overlapping or enlarging the field of typical layered intrusions as Bushveld and Stillwater, while the selected spinels and Cr-spinels from the Ronda massif plot separately, as corresponds to the spinel composition (higher #Mg and lower #Cr values). Therefore, to avoid confusion, the general information referred to this ultramafic province is here referred to as Málaga, while the specific information related to the Ojén or Ronda massifs is labelled by these local names. Fig. 1 further suggests that the Ojén chromitites are compositionally akin to the stratiform type, as part of a larger group; again to avoid confusion, this group will be referred to in the following text as the continental type, as distinct from the ophiolitic and from the metamorphosed types.

The chemical composition of all analysed grains was determined by electron-probe microanalysis (see Table 1) before the VNIR spectra measurements reported in Table 2. Compositional data were obtained using a CAMECA SX50 instrument in

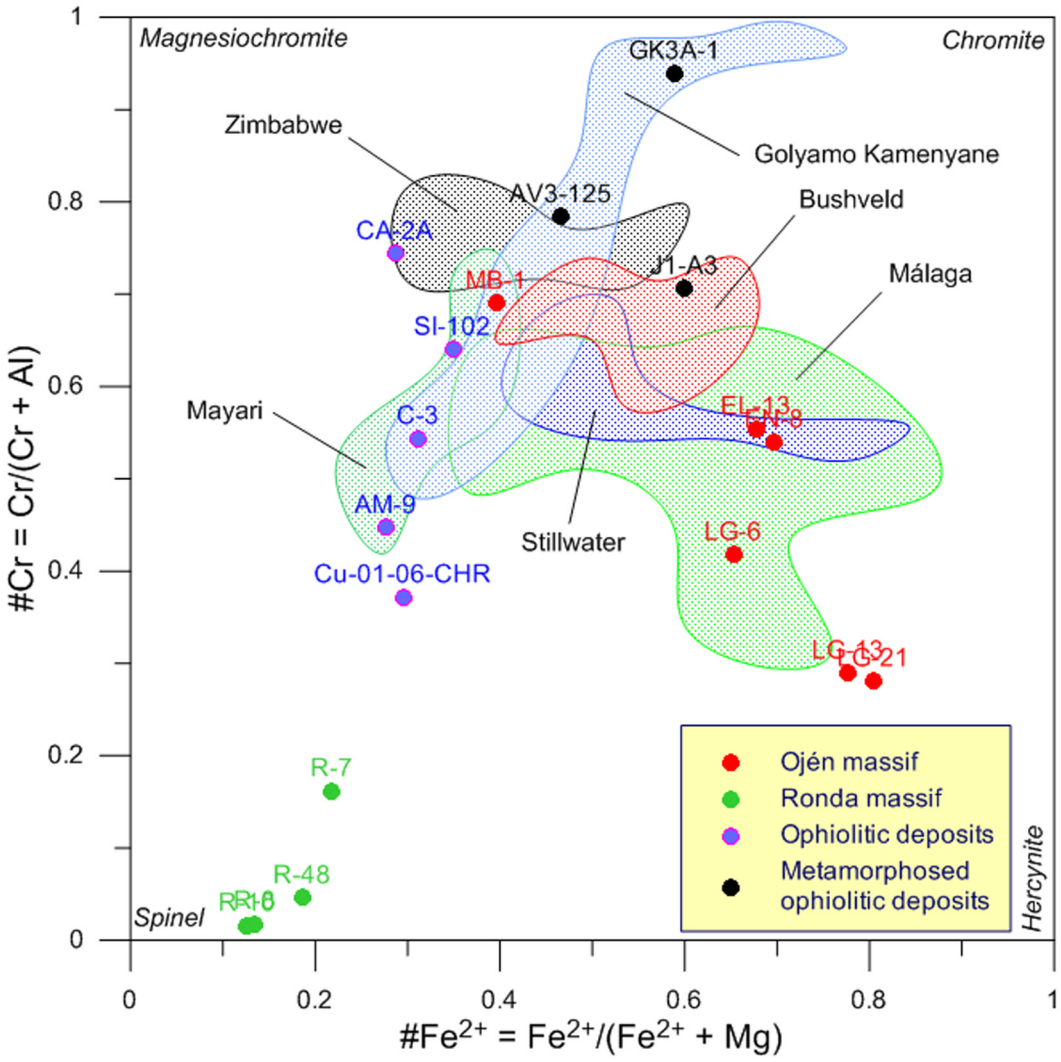

Fig. 1. Samples used in this study plotted on the base of the Haggerty spinel prism (#Fe^{2+} - #Cr plane) compared to published data of other world deposits: Stillwater (Lenaz et al., 2012), Bushveld (Naldrett et al., 2009), Zimbabwe (Zhou and Kerrich, 1992), Mayarí (González-Jiménez et al., 2011), Golyamo Kamenyane (Gervilla et al., 2012), Málaga (Gervilla and Leblanc, 1990).

wavelength dispersive mode, at the Serveis Cientifico-Técnics of the University of Barcelona (Spain). The analytical conditions were 20 kV excitation voltage, 20 nA sample current, and beam diameter of 3 μm. Counting times were 20 s on TAP/PET and 30 s on LiF crystals. ZAF corrections were mede online. The following spectral lines were monitored: Mg Kα, Al Kα, Si Kα with the TAP diffracting crystal, Ti Kα and Cr Kα with the PET diffracting crystal, and V Kα, Mn Kα, Fe Kα, Ni Kα and Zn Kα with the LiF diffracting crystal. The calibration was performed using natural and synthetic standards: periclase (Mg), Al_2O_3 (Al), Cr_2O_3 (Cr), Fe_2O_3 (Fe), diopside (Si), rutile (Ti), pure metalic V, rhodonite (Mn), NiO (Ni), and sphalerite (Zn). Fe_2O_3 contents were calculated assuming stoichiometry.

2.2. Equipment

The experimental work to determine the VNIR spectra was carried out in the Applied Microscopy Laboratory (Laboratorio de Microscopía Aplicada y Análisis de Imagen, LMA), installed in the School of Mines (Universidad Politécnica de Madrid, UPM). The CAMEVA System was built on an automated Leica DM6000M reflected light microscope, equipped with a DTA RPF16 filter wheel comprising 13 Melles Griot interference filters to measure from 400 to 1000 nm, in 50 nm intervals (40 nm FWHM); images were acquired with a Basler Scout scA1400fm digital video camera with IEEE-1394 interface. The calibration standards used to date are certified Ocean Optics STAN-SSH and STAN-SSL (for high and low reflectances, resp.). The geometric calibration of the equipment is carried out with a polka-dot NT46-461 beam splitter from Edmund Optics. A more detailed description of the equipment and a thorough discussion of the method can be found in Castroviejo et al. (2013) and Catalina and Castroviejo (2016).

2.3. Visible and Near-Infra-Red (VNIR) reflectance values

The VNIR multispectral reflectance values of the different ores were measured directly on the images acquired with CAMEVA, after checking their quality to prevent possible errors due to such features as zoning, porosity or silicate inclusions, which may be common in metamorphic chromites and Cr-spinels. A software application (Castroviejo et al., 2013), specifically conceived to perform spectral analysis of minerals on acquired images, is used to define rectangular regions of the appropriate size (any size chosen by the operator: $\geqslant$ 1 pixel, i.e. 0.3 μm × 0.3 μm for a 20× objective) to be measured on the grains selected. In each region the

Table 1
Averaged compositional data from electron microprobe analysis.

	AM-9		CA-2A		GK3A-1		R-7		R-8		R-10		R-48		Cu-01–06-CHR		C-3	
N	11		4		24		2		3		1		2		11		10	
Al_2O_3	30.72	(0.21)	12.78	(0.08)	2.58	(0.14)	54.35	(6.87)	67.99	(0.45)	68.53	(–)	64.35	(0.39)	36.19	(0.39)	24.90	(0.63)
Cr_2O_3	37.06	(0.32)	55.47	(0.35)	58.90	(1.45)	15.52	(7.06)	1.85	(0.14)	1.64	(–)	4.67	(0.08)	31.93	(0.29)	44.22	(0.59)
Fe_2O_3	3.27	(0.78)	4.29	(0.35)	9.36	(1.61)	n.d.	(–)	0.02	(0.02)	n.d.	(–)	n.d.	(–)	2.46	(0.37)	2.82	(0.21)
V_2O_3	0.17	(0.02)	0.09	(0.04)	0.20	(0.03)	n.d.	(–)	n.d.	(–)	n.d.	(–)	n.d.	(–)	n.d.	(–)	0.18	(0.06)
FeO	11.31	(0.72)	10.62	(0.17)	19.39	(0.69)	9.69	(1.34)	6.48	(0.33)	6.19	(–)	9.39	(0.09)	12.36	(0.30)	12.41	(0.36)
MgO	16.72	(0.64)	14.94	(0.21)	7.71	(0.53)	19.56	(1.34)	23.40	(0.43)	23.96	(–)	21.83	(0.68)	16.66	(0.21)	15.49	(0.25)
MnO	0.17	(0.02)	0.18	(0.02)	1.03	(0.06)	0.19	(0.06)	0.06	(0.04)	0.12	(–)	0.10	(0.08)	0.17	(0.04)	n.d.	(–)
NiO	0.19	(0.03)	0.19	(0.03)	0.14	(0.03)	n.d.	(–)	n.d.	(–)	n.d.	(–)	n.d.	(–)	n.d.	(–)	0.17	(0.02)
ZnO	n.d.	(–)	n.d.	(–)	n.d.	(–)	0.08	(0.02)	0.05	(0.08)	0.03	(–)	n.d.	(–)	n.d.	(–)	n.d.	(–)
TiO_2	0.36	(0.03)	0.14	(0.01)	0.14	(0.03)	0.08	(0.01)	0.01	(0.01)	0.02	(–)	0.07	(0.05)	0.29	(0.03)	0.17	(0.04)
Total	99.95	(0.91)	98.68	(0.49)	99.45	(0.81)	99.45	(0.28)	99.86	(0.22)	100.47	(–)	100.39	(0.86)	100.06	(0.47)	100.42	(0.31)
Cr	0.851	(0.008)	1.398	(0.008)	1.618	(0.048)	0.327	(0.156)	0.036	(0.003)	0.032	(–)	0.092	(0.003)	0.718	(0.006)	1.044	(0.019)
Ti	0.008	(0.001)	0.003	(0.000)	0.004	(0.001)	0.002	(0.000)	–	(–)	–	(–)	0.001	(0.001)	0.006	(0.001)	0.004	(0.001)
V	0.002	(0.000)	0.001	(0.001)	0.003	(0.000)	–	(–)	–	(–)	–	(–)	–	(–)	–	(–)	0.003	(0.001)
Al	1.052	(0.011)	0.480	(0.004)	0.106	(0.006)	1.692	(0.168)	1.974	(0.022)	1.969	(–)	1.896	(0.009)	1.213	(0.010)	0.876	(0.018)
Fe^{3+}	0.077	(0.018)	0.112	(0.009)	0.262	(0.044)	–		–		–		0.010	(0.010)	0.056	(0.008)	0.068	(0.005)
Fe^{2+}	0.277	(0.020)	0.285	(0.006)	0.573	(0.025)	0.215	(0.035)	0.134	(0.007)	0.126	(–)	0.186	(0.014)	0.296	(0.007)	0.313	(0.010)
Mn	0.004	(0.000)	0.005	(0.001)	0.030	(0.001)	0.004	(0.002)	0.001	(0.001)	0.002	(–)	0.002	(0.002)	0.004	(0.001)	–	(–)
Mg	0.723	(0.020)	0.710	(0.006)	0.399	(0.024)	0.770	(0.032)	0.859	(0.012)	0.870	(–)	0.813	(0.016)	0.706	(0.007)	0.689	(0.009)
Ni	0.004	(0.001)	0.005	(0.001)	0.004	(0.001)	–	(–)	–	(–)	–	(–)	–	(–)	0.004	(0.001)	–	(–)
Zn	–	(–)	–	(–)	–	(–)	0.001	(0.000)	0.001	(0.001)	0.001	(–)	–	(–)	–	(–)	–	(–)
#Cr	0.447	(0.002)	0.744	(0.002)	0.939	(0.004)	0.162	(0.078)	0.018	(0.001)	0.016	(–)	0.046	(0.001)	0.372	(0.003)	0.544	(0.010)
#Mg	0.723	(0.020)	0.713	(0.006)	0.411	(0.025)	0.782	(0.035)	0.865	(0.007)	0.873	(–)	0.813	(0.014)	0.705	(0.007)	0.688	(0.010)

	SI-102		MB-1		AV3-125		J1A-3		EL-13		EN-8		LG-6		LG-13		LG-21	
N	11		12		2		5		1		3		5		5		5	
Al_2O_3	18.82	(0.39)	15.86	(0.20)	10.63	(0.07)	14.49	(0.67)	22.54	(–)	22.93	(2.56)	30.89	(0.40)	38.82	(1.43)	38.,82	(1.43)
Cr_2O_3	49.98	(0.43)	52.66	(0.33)	57.55	(0.56)	52.03	(0.14)	41.68	(–)	40.29	(0.61)	33.17	(0.50)	22.61	(1.61)	22.,61	(1.61)
Fe_2O_3	2.69	(0.20)	2.69	(0.39)	3.47	(0.39)	2.68	(0.78)	0.33	(–)	2.34	(2.96)	0.39	(0.33)	0.63	(0.19)	0.,63	(0.19)
V_2O_3	0.15	(0.03)	0.10	(0.05)	0.13	(0.02)	0.11	(0.02)	1.25	(–)	0.98	(0.09)	1.30	(0.00)	1.90	(0.00)	1.,90	(0.00)
FeO	13.33	(0.42)	14.92	(0.12)	16.52	(0.20)	21.37	(0.19)	24.53	(–)	25.47	(0.83)	25.23	(0.53)	29.98	(0.40)	29.,98	(0.40)
MgO	14.04	(0.28)	12.75	(0.10)	10.70	(0.01)	8.02	(0.14)	6.63	(–)	6.33	(0.26)	7.60	(0.32)	4.80	(0.23)	4.,20	(1.22)
MnO	0.23	(0.04)	0.19	(0.04)	0.88	(0.01)	0.50	(0.05)	0.40	(–)	0.32	(0.01)	0.23	(0.04)	0.20	(0.03)	0.,20	(0.03)
NiO	0.18	(0.04)	0.27	(0.03)	0.03	(0.04)	0.02	(0.02)	n.d.	(–)	n.d.	(–)	n.d.	(–)	n.d.	(–)	n.d.	(–)
ZnO	n.d.	(–)	n.d.	(–)	n.d.	(–)	n.d.	(–)	0.57	(–)	0.50	(0.09)	0.38	(0.05)	0.46	(0.11)	0.,46	(0.11)
TiO_2	0.27	(0.02)	0.31	(0.02)	0.07	(0.00)	0.03	(0.02)	0.57	(–)	0.46	(0.12)	0.45	(0.05)	0.20	(0.04)	0.,20	(0.04)
Total	99.74	(0.23)	99.81	(0.28)	99.99	(0.41)	99.25	(0.31)	98.50	(–)	99.62	(0.34)	99.64	(0.45)	99.60	(0.13)	99.,00	(1.46)
Cr	1.226	(0.013)	1.318	(0.009)	1.490	(0.009)	1.359	(0.006)	1.073	(–)	1.025	(0.020)	0.810	(0.013)	0.547	(0.042)	0.554	(0.035)
Ti	0.006	(0.000)	0.007	(0.000)	0.002	(0.000)	0.001	(0.001)	0.014	(–)	0.011	(0.003)	0.010	(0.001)	0.005	(0.001)	0.005	(0.001)
V	0.002	(0.001)	0.002	(0.001)	0.002	(0.000)	0.002	(0.000)	0.020	(–)	0.015	(0.001)	0.019	(0.000)	0.028	(0.000)	0.028	(0.001)
Al	0.689	(0.012)	0.592	(0.008)	0.410	(0.001)	0.564	(0.025)	0.865	(–)	0.870	(0.093)	1.126	(0.016)	1.399	(0.045)	1.420	(0.080)
Fe^{3+}	0.068	(0.005)	0.071	(0.010)	0.092	(0.011)	0.072	(0.021)	–	(–)	0.051	(0.080)	0.005	(0.007)	–	(–)	–	(–)
Fe^{2+}	0.348	(0.012)	0.395	(0.004)	0.456	(0.003)	0.593	(0.006)	0.677	(–)	0.697	(0.019)	0.658	(0.015)	0.782	(0.007)	0.794	(0.022)
Mn	0.006	(0.001)	0.005	(0.001)	0.025	(0.000)	0.014	(0.001)	0.011	(–)	0.009	(0.000)	0.006	(0.001)	0.005	(0.001)	0.005	(0.001)
Mg	0.649	(0.011)	0.602	(0.003)	0.522	(0.002)	0.395	(0.006)	0.322	(–)	0.304	(0.014)	0.350	(0.015)	0.219	(0.011)	0.193	(0.053)
Ni	0.005	(0.001)	0.007	(0.001)	0.001	(0.001)	0.001	(0.001)	–	(–)	–	(–)	–	–	–	–	–	–
Zn	–	(–)	–	(–)	–	(–)	–	(–)	0.014	(–)	0.012	(0.002)	0.009	(0.001)	0.010	(0.003)	0.011	(0.003)
#Cr	0.640	(0.007)	0.690	(0.004)	0.784	(0.000)	0.707	(0.010)	0.554	(–)	0.542	(0.032)	0.419	(0.007)	0.281	(0.022)	0.281	(0.022)
#Mg	0.651	(0.012)	0.604	(0.003)	0.534	(0.003)	0.400	(0.006)	0.322	(–)	0.303	(0.016)	0.347	(0.015)	0.218	(0.010)	0.194	(0.050)

Oxides in wt%. Cations in apfu on the basis of 32 oxygens. #Cr = Cr/(Cr + Al). #Mg = Mg/(Mg + Fe^{2+}). N = number of measures. n.d.: not detected. In brackets: standard deviation. Samples: AM-9: Moa-Baracoa massif (Eastern Cuba); CA-2A: Mayarí massif (Eastern Cuba); GK3A-1: Golyamo Kemenyane serpentinite (Bulgaria); EL-13, EN-8, LG-6, LG-13, LG-21: Ojén ultramafic massif (Spain); R-7, R-8, R-10 and R-48: spinelite layers from Ronda ultramafic massif (Spain); Cu-01–06-CHR:Camagüey massif (Central Cuba); C-3 and SI-102: Sagua de Tánamo massif (Eastern Cuba); MB-1: Ojén ultramafic massif (Spain); AV3-125: Avren serpentinite (Bulgaria) and J1A-3: Yakovitsa serpentinite (Bulgaria).

average multispectral reflectance is computed and stored as a line in a text file for subsequent statistical treatment. A sufficiently large number of regions (usually $\geqslant 10$) was measured in each grain to check and warrant reproducibility.

3. Correlations between reflectance and chemical composition

We define the chromite composition on the basis of values of #Cr = Cr/(Cr + Al), #Mg = Mg/(Mg + Fe^{2+}) and #Fe^{3+} = Fe^{3+}/(Fe^{3+}+Cr + Al). Since we found that correlations between these three indices and reflectance at any wavelength in the range 400–1000 nm are similar, we use here only reflectance at 550 nm (R_{550}) because correlations at this wavelength are slightly better. As can be seen in Fig. 2, reflectance follows a linear trend with #Cr: increasing R values for samples with higher values of #Cr. However, the chromites from the three types of orebodies considered are grouped following parallels trends. Podiform chromites from ophiolitic massifs have lower reflectance than chromites from continental ores (Ojén massif) for the same #Cr value. Behaviour of metamorphosed chromites is intermediate. This fact may be related with the magnesium content (see Fig. 2) where two sample groups can be clearly distinguished: samples from podiform chromitites (blue circles) with the tendency of diminishing the Mg/Fe ratio as the reflectance increases and the samples from the Ojén ultramafic massifs (red circles) which have the opposite behaviour. Trends for #Fe^{3+} vs. reflectance are similar to those for #Cr vs. reflectance; however, this should be checked on samples with higher Fe^{3+} content since the compositions chosen for the present study are Fe^{3+}-poor. This behaviour mirrors in some way the compositional trends shown in Fig. 1. The sample MB-1

Table 2
Averaged VNIR reflectances (in %)

	Sample	AM-9		CA-2A		GK3A-1		R-7		R-8		R-10		R-48		Cu-01-06-CHR		C-3	
	N	37		35		26		32		36		39		35		39		40	
W	400	10.72	(0.16)	13.23	(0.28)	15.45	(2.76)	7.73	(0.19)	6.80	(0.00)	6.80	(0.00)	7.66	(0.14)	9.94	(0.15)	11.41	(0.20)
a	450	10.40	(0.00)	12.99	(0.22)	15.51	(3.37)	7.86	(0.19)	6.78	(0.09)	6.80	(0.00)	7.68	(0.16)	9.62	(0.09)	11.13	(0.15)
v	500	10.24	(0.20)	12.66	(0.19)	15.42	(2.82)	7.89	(0.18)	6.74	(0.14)	6.79	(0.06)	7.79	(0.20)	9.53	(0.16)	10.80	(0.00)
e	550	10.00	(0.00)	12.40	(0.17)	15.09	(2.76)	7.84	(0.20)	6.62	(0.20)	6.79	(0.06)	7.76	(0.20)	9.21	(0.06)	10.40	(0.00)
l	600	9.98	(0.09)	12.13	(0.19)	14.75	(2.69)	7.89	(0.18)	6.51	(0.18)	6.69	(0.18)	7.79	(0.20)	9.20	(0.00)	10.40	(0.00)
e	650	9.60	(0.00)	11.76	(0.20)	14.43	(2.65)	7.90	(0.18)	6.43	(0.11)	6.40	(0.00)	7.74	(0.19)	9.13	(0.16)	10.00	(0.00)
n	700	9.60	(0.00)	11.59	(0.07)	14.17	(2.59)	7.96	(0.12)	6.40	(0.00)	6.40	(0.00)	7.79	(0.20)	8.89	(0.17)	10.00	(0.00)
g	750	9.35	(0.20)	11.28	(0.16)	14.06	(2.59)	8.21	(0.20)	6.40	(0.00)	6.40	(0.00)	7.82	(0.24)	8.94	(0.19)	9.84	(0.20)
t	800	9.20	(0.00)	11.20	(0.00)	13.82	(2.57)	8.30	(0.18)	6.37	(0.11)	6.40	(0.00)	7.90	(0.34)	8.88	(0.16)	9.60	(0.00)
h	850	9.14	(0.15)	10.80	(0.00)	13.62	(2.56)	8.30	(0.18)	6.21	(0.20)	6.13	(0.19)	7.90	(0.34)	8.86	(0.15)	9.59	(0.06)
	900	8.80	(0.00)	10.73	(0.15)	13.57	(2.52)	8.29	(0.18)	6.13	(0.19)	6.09	(0.17)	7.89	(0.33)	8.83	(0.11)	9.42	(0.20)
(nm)	950	8.80	(0.00)	10.40	(0.00)	13.42	(2.56)	8.30	(0.18)	6.03	(0.11)	6.09	(0.17)	7.90	(0.34)	8.86	(0.15)	9.23	(0.14)
	1000	8.44	(0.13)	10.19	(0.20)	13.49	(2.55)	8.31	(0.20)	5.93	(0.20)	5.91	(0.17)	7.90	(0.34)	8.80	(0.09)	9.13	(0.15)
	Sample	SI-102		MB-1		AV3-125		J1-A3		EL-13		EN-8		LG-6		LG-13		LG-21	
	N	40		39		34		27		29		32		38		22		37	
W	400	12.15	(0.20)	12.70	(0.18)	14.71	(0.33)	13.97	(0.22)	12.94	(0.29)	12.78	(0.17)	11.60	(0.16)	10.93	(0.23)	10.75	(0.17)
a	450	11.95	(0.13)	12.33	(0.16)	14.52	(0.35)	13.67	(0.29)	12.77	(0.34)	12.64	(0.20)	11.40	(0.24)	10.93	(0.23)	10.50	(0.17)
v	500	11.59	(0.06)	11.97	(0.11)	14.19	(0.38)	13.23	(0.31)	12.43	(0.28)	12.38	(0.10)	11.11	(0.20)	10.75	(0.31)	10.27	(0.19)
e	550	11.22	(0.09)	11.61	(0.06)	13.79	(0.41)	12.77	(0.27)	12.11	(0.24)	12.00	(0.00)	10.97	(0.24)	10.47	(0.20)	10.10	(0.17)
l	600	11.06	(0.19)	11.31	(0.18)	13.38	(0.33)	12.52	(0.24)	11.83	(0.25)	11.81	(0.20)	10.75	(0.19)	10.36	(0.30)	10.00	(0.09)
e	650	10.79	(0.06)	11.20	(0.00)	12.94	(0.29)	12.16	(0.20)	11.60	(0.24)	11.59	(0.07)	10.60	(0.20)	10.07	(0.20)	9.84	(0.20)
n	700	10.62	(0.20)	10.82	(0.09)	12.65	(0.30)	11.87	(0.19)	11.35	(0.20)	11.23	(0.10)	10.36	(0.12)	9.89	(0.28)	9.62	(0.09)
g	750	10.41	(0.11)	10.80	(0.00)	12.48	(0.29)	11.76	(0.20)	11.20	(0.15)	11.18	(0.10)	10.27	(0.19)	9.69	(0.17)	9.60	(0.00)
t	800	10.34	(0.14)	10.42	(0.09)	12.18	(0.30)	11.51	(0.17)	10.94	(0.19)	10.84	(0.12)	10.14	(0.19)	9.64	(0.24)	9.52	(0.16)
h	850	10.22	(0.20)	10.40	(0.00)	11.96	(0.27)	11.42	(0.20)	10.79	(0.07)	10.71	(0.17)	10.00	(0.21)	9.33	(0.19)	9.29	(0.17)
	900	10.01	(0.11)	10.23	(0.20)	11.81	(0.30)	11.29	(0.17)	10.55	(0.20)	10.44	(0.12)	9.93	(0.26)	9.27	(0.20)	9.22	(0.09)
(nm)	950	9.96	(0.12)	10.01	(0.06)	11.56	(0.27)	11.14	(0.14)	10.39	(0.07)	10.31	(0.17)	9.92	(0.32)	9.11	(0.24)	9.05	(0.20)
	1000	9.72	(0.21)	9.78	(0.20)	11.25	(0.24)	10.84	(0.13)	10.11	(0.18)	9.91	(0.17)	9.58	(0.31)	8.87	(0.20)	8.83	(0.11)

N is the number of regions measured. In brackets: standard deviations.

shows an exceptional composition, with #Fe^{2+} values lower (or #Mg values higher) than the expected value for continental ores (Fig. 1). However it plots correctly in the continental trend in Fig. 3, for compositions deduced from reflectance measures.

We have also investigated the possible correlations between the VNIR reflectance spectra (Table 2) and the compositional data (Table 1). Hereafter it is important to bear in mind that reflectance is given in percentage for a range of wavelengths between 400 and 1000 nm, that compositional values are given in apfu (atoms per formula unit) on the basis of a 32-oxygen chromite formula and that #Cr, #Fe2 + and #Mg are dimensionless numbers. When it was possible, the treatment was made separately for each type of studied orebody, considering the reflectance at different wavelengths (λ).

3.1. Coefficients of correlation

The matrix of Pearson's coefficients of correlations is important, because multiple linear regression analysis is based on the hypothesis that regressor variables are uncorrelated (the matrix of coefficients of correlation has non zero determinant). If this assumption is not met, the least square system of equations has

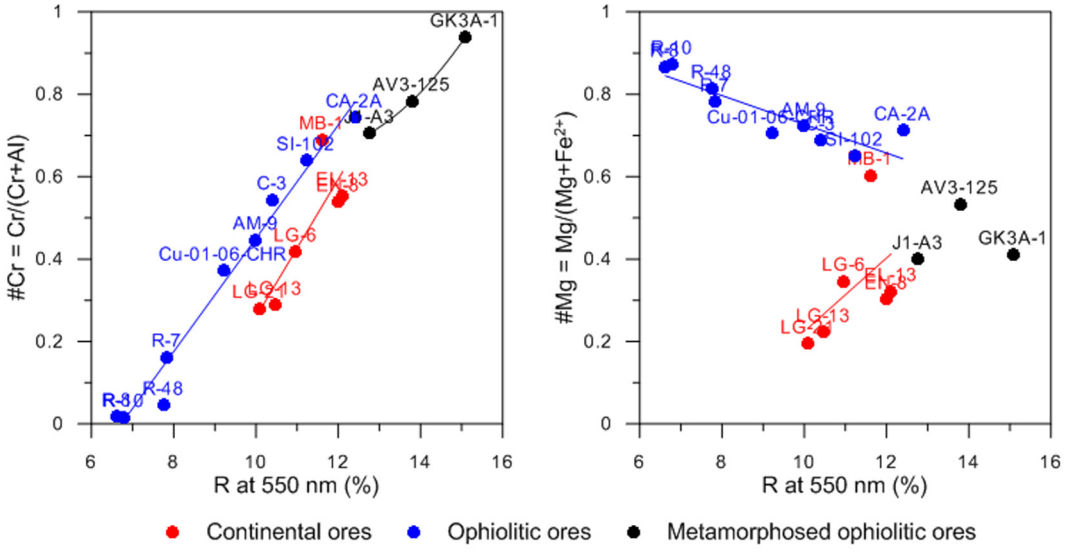

Fig. 2. Plot of #Cr and #Mg vs. reflectance at 550 nm.

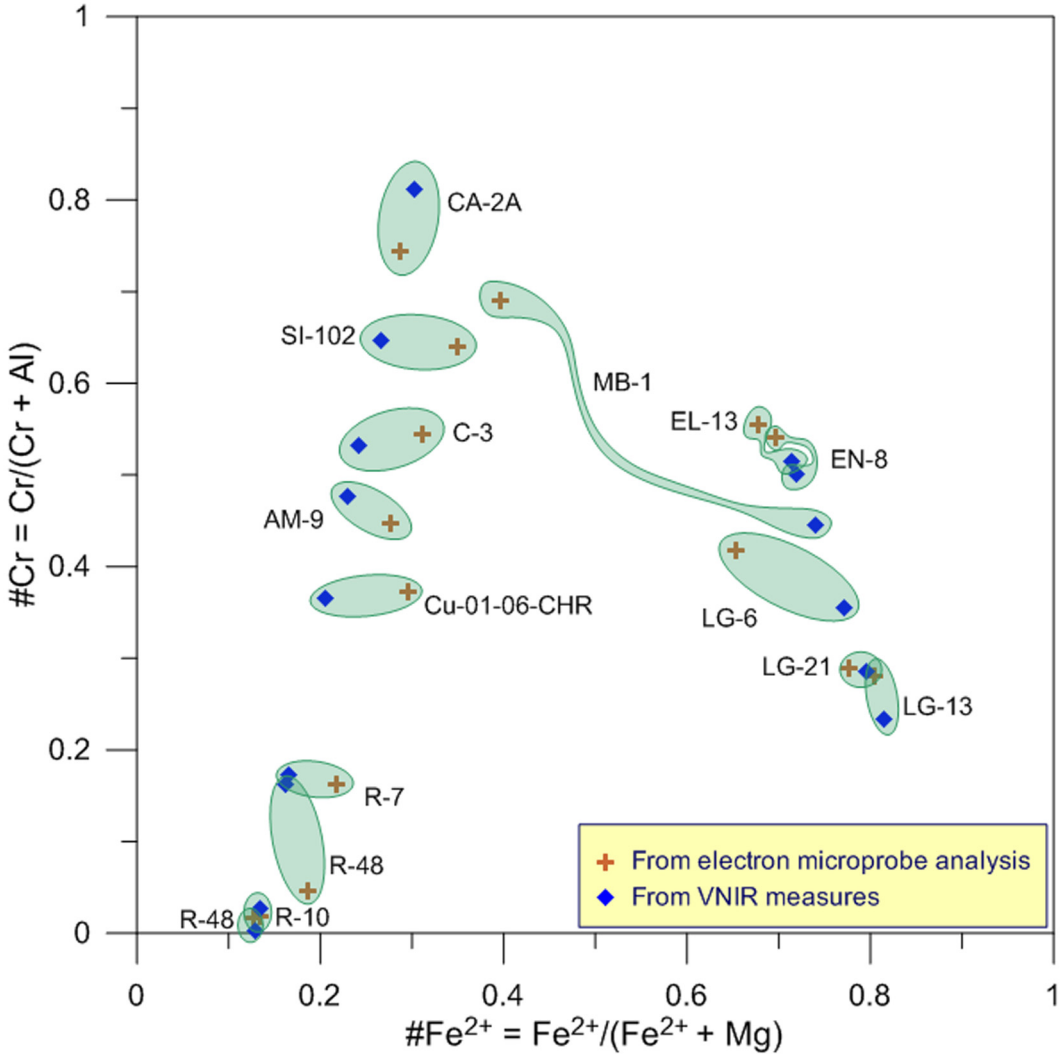

Fig. 3. Comparison of the values of #Cr and #Fe2 + calculated from compositional data and estimated from their correlations with reflectance at 550 nm (see Fig. 2 also).

a non-unique solution and the collinearity effect appears. As a result, the validity of the linear regression analysis can become highly questionable (see for example Rawlings et al. (2001)).

For the variables Cr, Ti, Al, V, Fe^{3+}, Fe^{2+}, Mn, Mg, Ni and Zn the most relevant linear correlations are obviously Cr–Al and Mg–Fe^{2+}, due to the fact that, for the compositions chosen (near the base of the Hagerty prism) and given the spinel stoichiometry, Cr + Al ≈ 2 and Mg + Fe^{2+} ≈ 1. Therefore, care has been taken in the forthcoming linear regression analysis to avoid putting together either Cr and Al, or Mg and Fe^{2+}. Samples EN-8, LG-21 and R-10 were reserved as control samples, and the analysis was performed on the remaining samples.

3.2. Reflectance vs. chemical composition

As it was previously explained, Fig. 2 shows a good correlation between #Cr and #Mg and reflectance at 550 nm for podiform and continental chromite ores, as well as for the Ronda spinelites. This allows to estimate the values of #Cr and, more loosely, #Mg of the non-metamorphosed samples used in this study:

- Ophiolitic ores:

$$\#Cr = -0.92 + 0.14R_{550}, \quad r^2 = 0.9768$$
$$\#Mg = 1.07 - 0.03R_{550}, \quad r^2 = 0.7809$$

- Continental ores:

$$\#Cr = -1.18 + 0.14R_{550}, \quad r^2 = 0.9731$$
$$\#Mg = -0.32 - 0.05R_{550}, \quad r^2 = 0.5519$$

where r^2 is the *coefficient of determination*.

Fig. 3 shows a good concordance of the #Cr and #Mg values estimated by these correlations and calculated from the compositional data. Again, sample MB-1 appears as an anomalous case.

There are different ways to select the independent variables that a regression model must include. Most popular are the so-called stepwise selection methods. In these methods, variables are included sequentially in the order defined by such statistical criteria as the value of the coefficient of determination or the value of the coefficient of partial correlation. The process stops when the addition of any new variable does not improve the regression model (see for example Rawlings et al. (2001)).

Multiple linear regression analysis of reflectance measured for each studied wavelength vs. chemical composition (apfu) leads to linear models that depend strongly on the Cr content (for wavelengths of 400 and 450 nm) or the Al content (for wavelengths longer than 450 nm). To a lesser extent, Mg and Mn contents also contribute to the definition of the regression hyperplane. In these models, the relative contributions of these elements to the

Table 3
Standardized (to zero mean and unit standard deviation) regression coefficients for the models $R_\lambda = A \cdot Cr + B \cdot Al + C \cdot Mg + D \cdot Mn$ (*).

Wavelength (nm)	r^2	A	B	l	D
400	0.988	0.796	–	−0.211	0.119
450	0.988	0.750	–	−0.217	0.173
500	0.987	–	−0.730	−0.227	0.188
550	0.983	–	−0.710	−0.227	0.210
600	0.982	–	−0.719	−0.227	0.199
650	0.984	–	−0.704	−0.231	0.214
700	0.976	–	−0.703	−0.212	0.227
750	0.975	–	−0.674	−0.202	0.268
800	0.962	–	−0.653	−0.197	0.289
850	0.959	–	−0.660	−0.182	0.291
900	0.947	–	−0.630	−0.182	0.318
950	0.936	–	−0.607	−0.184	0.337
1000	0.899	–	−0.597	–	0.446

r^2 is the coefficient of determination.
* Cations in apfu on the basis of 32 oxygens.

reflectance varies with the wavelength (see Fig. 6): as the wavelength increases, the contribution of Cr and Al decreases, and that of Mn increases, while the importance of Mg remains more or less constant. It is remarkable that the model for $\lambda = 1000$ nm does not depend on the Mg content.

In all cases, Student's t-distribution based tests of coefficients nullity reveal that all the regression coefficients are non-zero at a level of confidence of 0.05, so all regressions are significant. Determination coefficients, r^2, are near to unity, thus low dispersion around the regression hyperplane is expected.

As a general trend, model fits for the shorter wavelengths are better than those for longer wavelengths, as pointed out by the variations of the coefficient of determination, r^2, decreasing as the wavelength increases. Table 3 gives the regression results. In Fig. 4, the measured and predicted reflectance values are plotted. Fig. 5 is a comparison of the measured and predicted VNIR reflectance spectra for the control samples. Both figures show in general a very good agreement, allowance being made for VNIR values in sample R-10. This sample can be regarded as an almost predictable exception, given the almost pure spinel composition of the ore and its high transparency, usually producing frequent internal reflections which may interfere with the reflectance measures. In Fig. 6, the contributions of Cr, Al, Mg and Mn to the r^2 coefficient and to the regression hyperplane are displayed.

3.3. Models for VNIR reflectance

The fit of several known models (linear, exponential, logarithmic, ...) to the VNIR reflectance spectra of the samples included in this study was tried. The best fits were obtained for the second order polynomial model:

$$R = \alpha + \beta\lambda + \gamma\lambda^2$$

with values of the coefficient of determination very close to unity. The results of these fits can be seen in Table 4. Fig. 7 shows some examples of these fits compared with the measured spectra.

Correlation between coefficients α, β and γ of the second order polynomials fit and the chemical composition of the samples was also investigated. Fig. 8 shows some of these correlations, plotted against #Cr. It can be seen that the trend of coefficient α is to increase as chrome content increases while that of coefficient β is just the opposite. Coefficient γ seems to be independent of chrome content, i.e. the curvature of all the fitting polynomials is almost identical. Best fits correspond to the second order polynomials:

$$\alpha = 6.556 + 17.479\#Cr + 0.468\#(Cr)^2, \quad r^2 = 0.915$$
$$\beta = 0.703 - 15.658\#Cr + 2.797\#(Cr)^2, \quad r^2 = 0.703$$
$$\gamma = -0.923 + 8.999\#Cr - 5.090\#(Cr)^2, \quad r^2 = 0.538$$

4. VNIR multispectral analysis, chromite composition and deposit typology: a discussion

The information shown in Figs. 2 and 7 suggests that VNIR multispectral values of chromite are related to the mineral's composition and also dependent on ore deposit environment. However, this relationship is complex, as can be expected from the variability and complexity of the crystal chemistry of the ore, as part of the spinel family. Actually, purely theoretical, stoichiometric chromite compositions ($FeCr_2O_4$) are only rarely if ever found in nature. Instead, chromites containing variable amounts of Mg, Al, and Fe^{3+} (among other metals, such as Mn, Ni, Zn or Ti, present usually in minor amounts) are commonly found. Even if there is a relationship of each metal content and the reflectance value, this is obscured by the fact that the resulting value (measured reflectance) depends also on other metals present, and these may have an effect contrary to that of the element considered. However, as Fig. 8 shows, an indirect calculation of composition based on VNIR reflectance data is possible, through compound compositional values which can be deduced from the model fit (e.g. #Cr in Fig. 8), and which may provide relevant information to exploration geologists, to process engineers and to metallurgists. To obtain a complete compositional information, a larger chromite population with systematic compositional variations should be studied; the results obtained so far suggest that this aim might be attained through multispectral reflectance analysis.

On the other hand, comparison of Figs. 1 and 2 suggests a relationship of a general character between chromite compositions and ore deposit type or environment, and this relationship seems to be also displayed in reflectance-compositional plots. In Fig. 2, monochromatic (550 nm) reflectance values are plotted against compositional values represented by #Cr and #Mg numbers. In both cases, all values follow linear trends, with the only exception of the #Mg in chromites from metamorphosed ophiolitic deposits (AV3-125, GK3-A1, J1-A3), whose dispersion might be anticipated, e.g. by Mg mobility and/or Fe oxidation during metamorphism. However the interesting point is that the three deposit types to which the three groups of samples chosen for this study belong can be identified in the diagrams. The values from each deposit environment group together and plot in the R-composition space in a specific region which differs from the other types of deposits (with the only exception of the sample MB-1, which belongs to

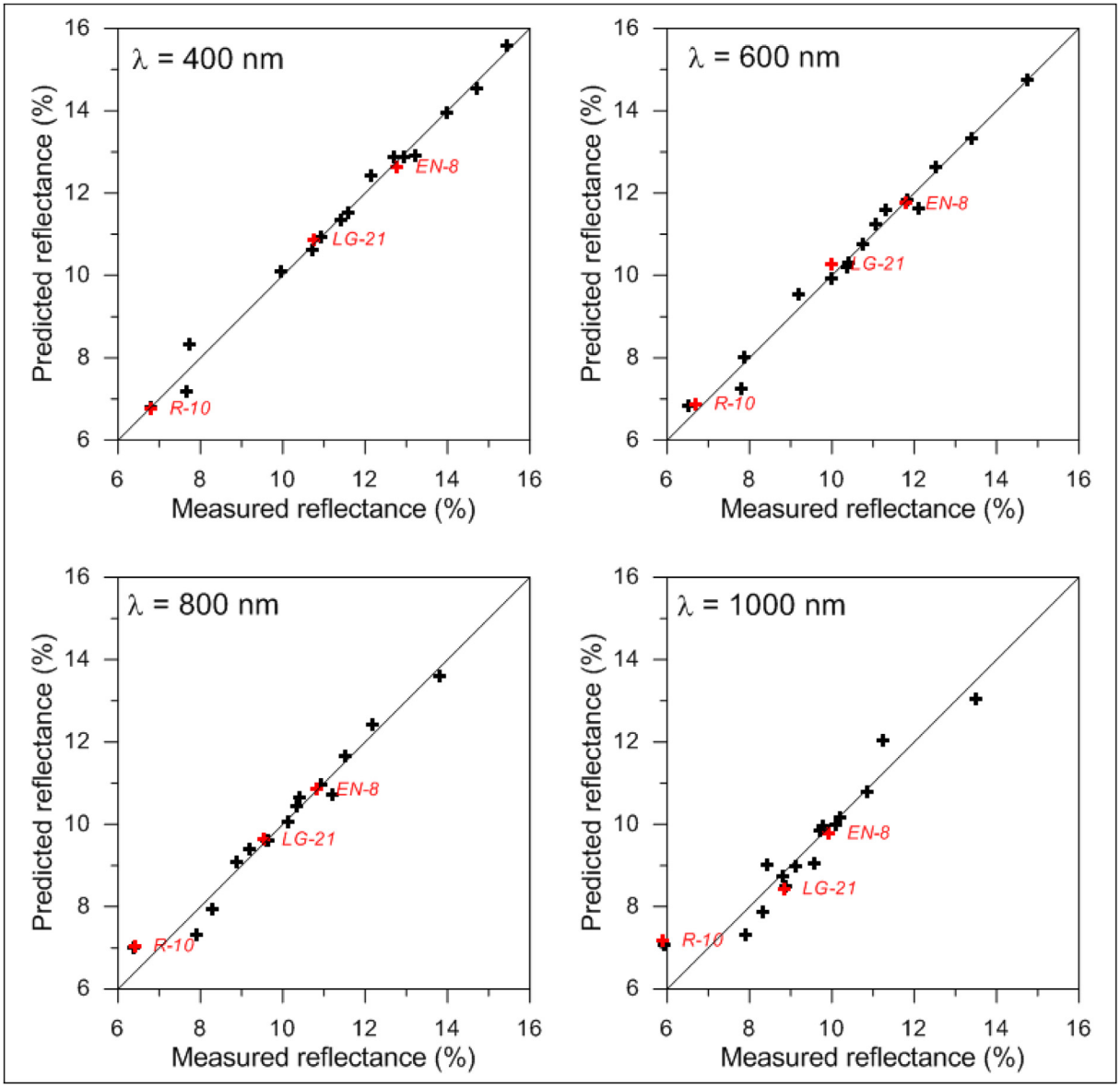

Fig. 4. Plots of predicted vs. measured reflectance at 400, 600, 800 and 1000 nm. Predictions are made with the models of Table 3. In red, the control samples. As the increasing values of r^2 suggest, dispersion increases for longer wavelengths (1000 nm).

the Ojén massif but plots near the ophiolitic trend). Although there is no obvious and inequivocal explanation for the behaviour of sample MB-1, it might be due to this sample's anomalous composition (Fig. 1) and particularly to its Ni content of 0.27 %, by far the highest of all the ores analysed (Table 1); unfortunately, the influence of this metal on R could not be duly quantified in this work, since Ni content of most samples is below the analytical detection limit (Table 1). On the other hand, MB-1 compositions calculated from the measured reflectance values plot correctly within the continental type field (Fig. 3). The Ronda spinelites also plot separately in the low R, low #Cr and high #Mg corner and they seem to be aligned with the ophiolitic trend. However, the compositional gap separating both groups precludes any reliable explanation until further samples with known genesis and appropriate composition are analysed.

These results suggest a practical application for exploration: to define a reflectance-based rule to predict the type of orebody (ophiolitic or continental) from which a sample comes, so that the exploration geologist might gain this information from few

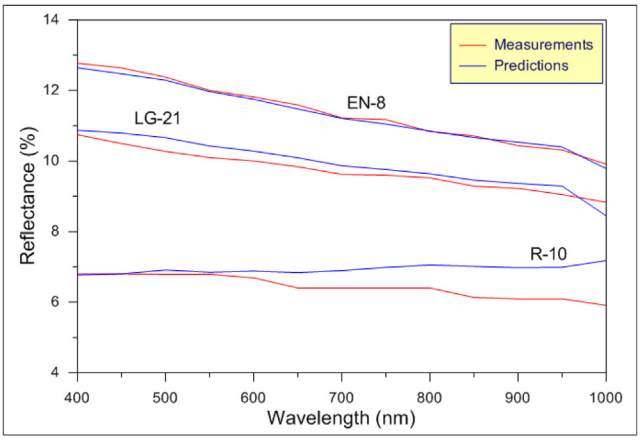

Fig. 5. The VNIR spectra of the control samples. Predictions of models of Table 3 become worse for the longest wavelength and for the samples with lower reflectance (near spinel compositions).

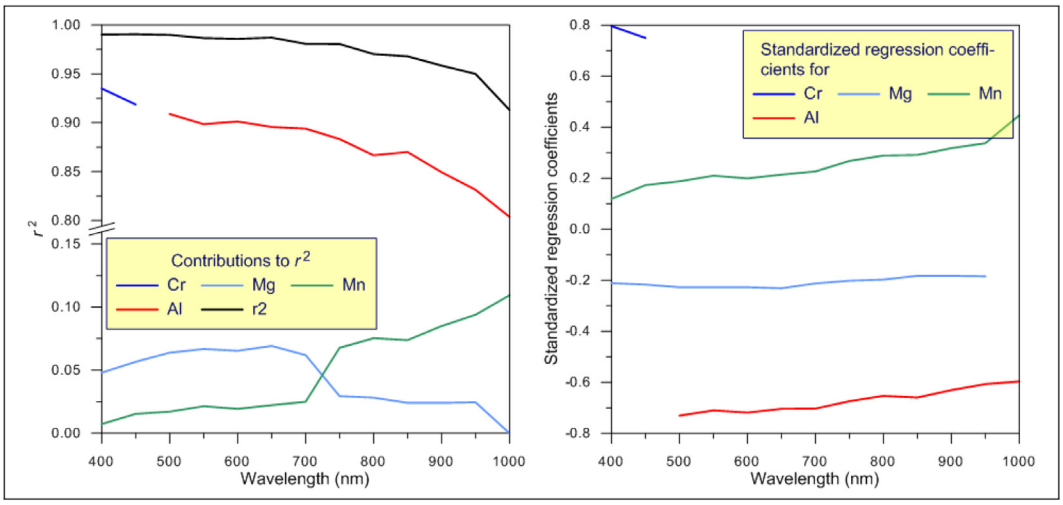

Fig. 6. Contributions of Cr, Al, Mg and Mn to the regression hyperplanes defined in Table 3 (right) and to the r^2 coefficient of this same models (left).

Table 4
Second order polynomial fitting the mean VNIR reflectance spectra ($R = \alpha + \beta \cdot \lambda + \gamma \cdot \lambda^2$).

Sample	α	β	γ	r^2
EL-13	15.6660	−7.5394	2.0446	0.9977
EN-8	15.0300	−5.8385	0.8114	0.9944
LG-6	13.8440	−6.6239	2.4777	0.9913
LG-13	12.6100	−4.0668	0.3475	0.9912
LG-21	12.2520	−4.3697	1.0372	0.9889
MB-1	16.0670	−10.1460	3.9618	0.9929
CA-2A	15.9620	−7.4461	1.7039	0.9968
SI-102	15.3220	−9.4752	3.9682	0.9939
C-3	14.2690	−8.7424	3.6633	0.9867
AM-9	10.8320	−0.1941	0.0014	0.9866
Cu-01–06-CHR	12.2780	−7.7478	4.3353	0.9730
R-7	7.2535	1.2313	−0.1077	0.8763
R-8	7.1760	−0.7099	−0.5081	0.9772
R-10	7.1385	−0.3516	−0.8657	0.9419
R-48	7.3847	0.8517	−0.3267	0.8469
GK3A-1	18.5030	−8.1245	2.9562	0.9704
J1-A3	18.5360	−13.2730	5.9019	0.9942
AV3-125	18.6190	−10.8960	3.5932	0.9948

r^2 is the coefficient of determination.

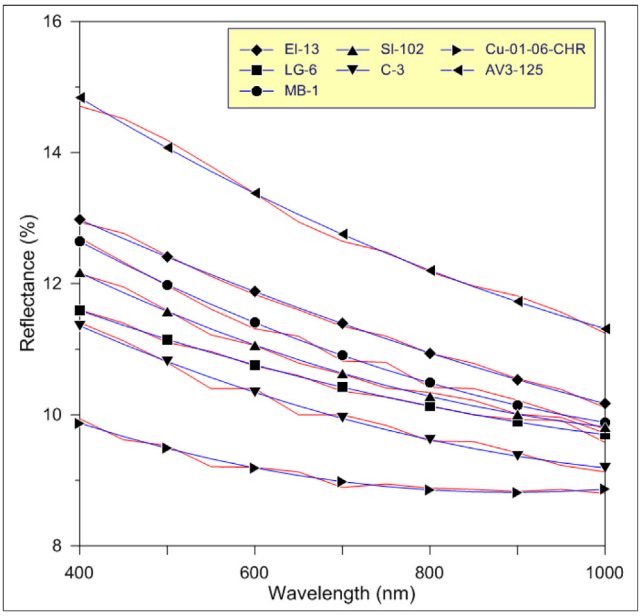

Fig. 7. Some examples of second order polynomial fit to the VNIR reflectance spectra. Red lines represent the measured spectra while the blue lines represent the modelized spectra.

samples, even if the orebody does not outcrop (e.g. drill cores from blind orebodies, placer occurrences, etc.). Statistics provides a tool, the *factorial discriminant analysis*, to perform this task. It is a technique for classifying a realization of a multivariate random variable from a sample into a predetermined group (see McLachlan, 2004). This method works looking for a set of linear functions called *canonical discriminant functions*, each one of them able to separate two groups. For example, if it is desired that discriminant function $\Phi = \sum_{j=1}^{k} b_j x_j$ be able to discriminate between two groups, the coefficients b_j are chosen in a way that the scores of Φ be maximum for individuals belonging to one of the groups and minimum for the other. Once the canonical discriminant functions has been computed, it is possible to use the Bayes' rule to compute the probability of an individual with observed attributes **X** of belonging to each group.

In this treatment we used as attributes the reflectances at different wavelengths looking for a function that discriminate between chromites from ophiolitic deposits (group 1) and chromites from continental deposits (group 2). Using the stepwise modality of discriminant analysis, the canonical discriminant function obtained was:

$$\Phi = -7.998R_{500} - 3.121R_{600} + 13.121R_{650} + 3.041R_{750} - 4.873R_{1000}$$

which has the averaged values −0.471 for the group 1 and 1.020 for the group 2.

To see how well the function Φ discriminates between the two groups it is customary the use of the statistic Wilk's Λ which is the ratio between the variance explained by the grouping and the total variance, and allows to test if the means of the two groups are equal or not. In this study, the value of this statistic is relatively high (0,672) indicating that, although the hypothesis of equality of means for the two groups can be rejected, a large interval of uncertainty should be expected (see Fig. 9).

There is a significant amount of misclassified samples: 11.9% of samples from ophiolitic chromitites are classified as continental while 39.1% of samples from continental chromitites are classified as ophiolitic. All those results lead to the conclusion that a

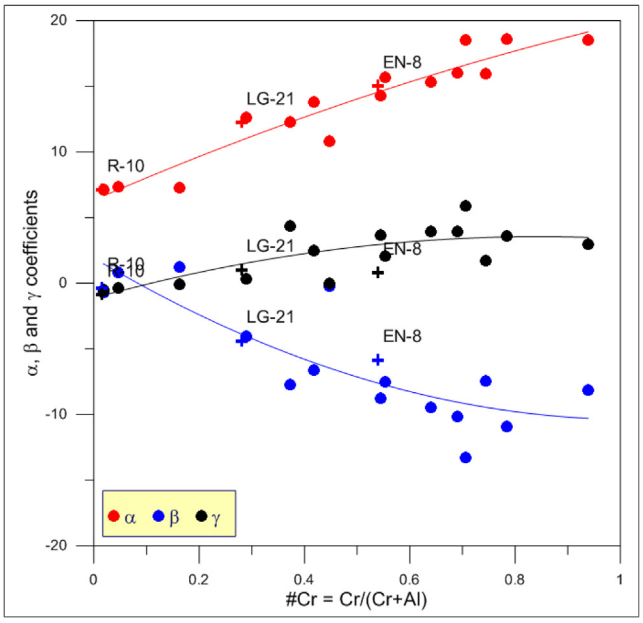

Fig. 8. Correlation between the coefficients α, β and γ of the second order polynomial fitted to the VNIR reflectance spectra and the #Cr. Control samples are represented by crosses.

classifier based on function Φ is poorly efficient. However, this analysis gives a valuable knowledge about the role played by the reflectance to predict from which type of orebody comes a sample. Since positive Φ values seem to be more likely to correspond to samples from continental ores while samples from ophiolitic ores seems to lead to negative Φ values (see Fig. 9)); and since reflectance at 650 nm values is the more determinant variable (largest positive coefficient) to obtain positive Φ values and reflectance at 500 nm values is the more determinant variable (largest negative coefficient) to obtain negative Φ values, we can conclude that samples with high reflectance at 650 nm are more likely to come from continental chromitite deposits while samples with high reflectance at 500 nm is more likely to come from ophilitic chromitite deposits. Chromites from metamorphosed ophiolitic deposits are in the range of Φ from −1.22 to 1.55, i.e. values in the region of largest uncertainty.

5. Concluding remarks

The experimental results presented show that the specular reflectance of chromite is related to the composition of the ore (Fig. 2 and 3). This relationship is necessarily complex, given the multiplicity of components and coupled substitutions observed in natural chromites (or Cr-spinels). Therefore a simple and direct, bi-univocal, determination is not to be expected. Nevertheless, the relationship can be conveniently expressed in terms of compositional parameters, such as #Cr = Cr/(Cr + Al) or #Mg = Mg/(Mg + Fe^{2+}) (alternatively, #Fe^{2+} = Fe^{2+}/(Mg + Fe^{2+}) = 1 − #Mg), and selected monochromatic reflectance values or intervals in the VNIR realm (e.g. 550 nm).

Statistical analysis suggests a good fit of the multispectral reflectance values to a second order polynomial model (Fig. 7), with a sound agreement between measured and predicted values, tested on independent trial samples (Figs. 3 and 4). It was also possible to predict with an acceptable accuracy the values of the coefficients of the fitting polynomials from the #Cr. These predictions are poorer for the samples from Ronda spinelites, probably because of their transparency and frequent internal reflections, whose interference with the specular reflected light may cause anomalous values of reflectance.

As it is known from literature (Eales, 1980), reflectance increases with increasing Fe^{3+} contents, therefore, to study the influence of other metals, low Fe^{3+} samples have been selected. Our results show that R increases with increasing #Cr while the effect of #Mg seems to be specific of the deposit type: increasing for the continental ores and decreasing for the ophiolitic ores. Nickel may be also significant, but its influence could not be quantified, since most of the samples studied had Ni contents below the detection limit.

Further refinements are to be expected if a larger Cr-spinel compositional population is analysed. However these preliminary results suggest that this method can provide to the geologist or the mining engineer a valuable information which can be already acquired in the early stages of exploration (e.g. from alluvial concentrations or from drillcore intersections of blind orebodies). First, chromite compositions can be estimated from multispectral reflectance values measured on polished sections of the ore, through the determination of the α, β, and γ coefficients of the second order polynomial model (Fig. 8, see also Fig. 3). Furthermore, as shown in Fig. 2, reflectance values can also give a hint to the

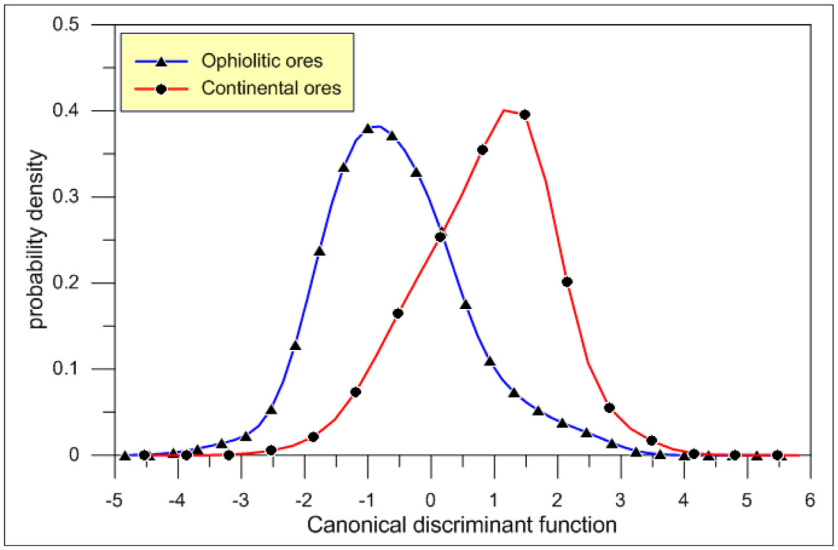

Fig. 9. Probability density function (pdf) of the canonical discriminant function for the two types of orebodies considered.

deposit environment or type (e.g. ophiolitic vs. metamorphosed vs. continental types), although a significant uncertainty cannot be excluded, particularly for metamorphosed deposits (Fig. 9); this means that this information should not be sought in single samples, but at best in sets of samples (e.g. several intersections from drill cores, several concentrates from heavy sands). Further studies, relating deposit typology, accurate ore composition and multispectral specular reflectance of chromite, would be instrumental to build an expanded data base, and might provide a sound basis to test and refine these preliminary conclusions.

References

Barnes, S.J., Roeder, P.L., 2001. The range of spinel compositions in terrestrial mafic and ultramafic rocks. J. Petrol. 42 (12), 2279–2302.

Bernhardt, H.J., 1987. A simple, fully-automated system for ore mineral identification. Mineral. Petrol. 36, 241–245.

Brea, C., Castroviejo, R., Samper, J., 2010. New data on the specular reflectance of ores (vnir: 400–1000 nm) and their significance for ore microscopy. In: Pál-Molnár, E. (Ed.), Acta Mineralogica-Petrographica (Proceedings of the IMA2010 Meeting). Budapest, Hungary (21–27 August, 2010), p. 281.

Carli, C., Sgavetti, M., 2011. Spectral characteristics of rocks: effects of composition and texture and implications for the interpretation of planet surface compositions. ICARUS 211, 1034–1048.

Castroviejo, R., Brea, C., Pérez-Barnuevo, L., Catalina, J.C., Segundo, F., Bernhardt, H.J., Pirard, E., 2009. Using computer vision for microscopic identification of ores with reflected light: preliminary results. In: Williams, P.J., et al. (Eds.), Smart Science for Exploration and Mining (Proceedings of the Tenth Biennial SGA Meeting). Townsville, Australia (17–20 August, 2009), vol. 2, pp. 682–684.

Castroviejo, R., Catalina, J.C., Bernhardt, H.J., Pirard, E., Segundo, F., Brea, C., Pérez Barnuevo, L., 2010. A fully automated system for multispectral ore microscopy. In: Pál-Molnár, E. (Eds.), Acta Mineralogica-Petrographica (Proceedings of the IMA2010 Meeting). Budapest, Hungary (21–27 August, 2010), p. 281.

Castroviejo, R., Espí, J.A., Brea, C., Pérez-Barnuevo, L., Catalina, J.C., Segundo, F., 2013. Patente de invención con examen previo: Método para obtener imgenes multiespectrales de reflectancia absoluta, patent ES 2 368 321 b2 (appl. n p201130499).

Castroviejo, R., Catalina, J.C., Bernhardt, H.J., Pirard, E., Brea, C., Pérez-Barnuevo, L., Segundo, F., Espí, J., 2014. Multispectral (visible and near infra-red, 400–1000 nm range) reflectance data file from common ore minerals. Data Base at IMA-COM web site: http://projects.gtk.fi/com/results/reflectancedata.html.

Catalina, J.C., Castroviejo, R., 2016. Microscopía de reflectancia multiespectral: aplicación al reconocimiento automatizado de menas metálicas. Rev. Metalurgia (submitted).

Clark, R.N., King, T.V.V., Klejwa, M., Swayze, G., Vergo, N., 1990. High spectral resolution reflectance spectroscopy of minerals. J. Geophys. Res. 95, 12653–12680.

Cloutis, E.A., Sunshine, J.M., Morris, R.V., 2004. Spectral reflectance-compositional properties of spinels and chromites: implications for planetary remote sensing and geothermometry. Meteorit. Planet. Sci. 39 (4), 545–565.

Cloutis, E.A., Klima, R.L., Lindsay, K., Coradini, A., Golubeva, L.F., McFadden, L.A., Shestopalov, D.I., Vilas, F., 2010. The 506 nm absorption feature in pyroxene spectra: nature and implications for spectroscopy-based studies of pyroxene-bearing targets. ICARUS 207, 295–313.

Colas, V., González-Jiménez, J.M., Griffin, W.L., Fanlo, I., Gervilla, F., O'Reilly, S.Y., Pearson, N.J., Kerestedjian, T.N., Proenza, J.A., 2014. Fingerprints of metamorphism in chromite: new insights from minor and trace elements. Chem. Geol. 389, 137–152.

Criddle, A., 1998. Ore microscopy and photometry. In: Cabri, L.J., Vaughan, D.J. (Eds.), Modern Approaches to Ore and Environmental Mineralogy. vol. 27 of MAC Short Course Series. pp. 1–74.

Criddle, A.J., Stanley, C.J. (Eds.), 1993. Quantitative data File for Ore Minerals. 3rd edition. Chapman & Hall, London.

Eales, H.V., 1980. The application of reflectivity measurements to the study of chromiferous spinels. Can. Mineral. 18, 17–23.

Freund, H. (Ed.), 1966. Applied ore microscopy: Theory and Technique. McMillan, N. York.

Gervilla, F., Leblanc, M., 1990. Magmatic ores in high-temperature alpine-type lherzolite massifs (Ronda, Spain, and Beni Bousera, Morocco). Econ. Geol. 85 (1), 112–132.

Gervilla, F., Padrón-Navarta, J.A., Kerestedjian, T.N., Sergeeva, I., González-Jiménez, J. M., Fanlo, I., 2012. Formation of ferrian chromite in podiform chromitites from the Golyamo Kamenyane serpentinite, Eastern Rhodopes, SE Bulgaria: a two stage process. Contrib. Miner. Petrol. 164, 647–657.

González-Jiménez, J.M., Proenza, J.A., Gervilla, F., Melgarejo, J.C., Blanco-Moreno, J. A., Ruiz-Sánchez, R., Griffin, W.L., 2011. High-Cr and high-Al chromitites from the Sagua de Tánamo district, Mayarí-Cristal Ophiolitic Massif (eastern Cuba): constrains on their origin from mineralogy and geochemistry of chromian spinel and platinum-group elements. Lithos 125 (1–2), 101–121.

Haggerty, S., 1976. Opaque mineral oxides in terrestrial igneous rocks, oxide minerals, short course notes, 3 d. Rumble III, Mineralogical Society of America, Washington, DC, Hg–101–Hg–277.

Henares, S., Gervilla, F., González-Jiménez, J.M., Proenza, J.A., Chang-Rodríguez, A., González-Pontón, R.B., 2010. Las cromititas del Complejo Ofiolítico de Camagüey, Cuba: un ejemplo de cromitas ricas en Al. Boletín de la Sociedad Geológica Mexicana 62, 173–185.

Lenaz, D., Garuti, G., Zaccarini, F., Cooper, R.W., Princivalle, F., 2012. The stillwater complex chromitites: the response of chromite crystal chemistry to magma injection. Geologica Acta 10 (1), 33–41.

López-Benito, A., Gervilla, F., Catalina, J.C., Castroviejo, R., 2015. Determination of chromite composition from multispectral reflectance measurements (400–1000 nm). In: André-Mayer, A., Cathelineau, M., Muchez, P., Pirard, E., Sindern, S. (Eds.), Mineral Resources in a Sustainable World (Proceedings of the 13th SGA Biennial Meeting). Nancy, France (24–27 August 2015), vol. 4, pp. 1435–1438.

McLachlan, G., 2004. Discriminant Analysis and Statistical Pattern Recognition. Wiley, Hoboken, New Jersey.

Naldrett, A.J., Kinnaird, J., Wilson, A., Yudovskaya, M., McQuade, S., Chunnett, G., Stanley, C., 2009. Chromite composition and PGE content of Bushveld chromitites: Part 1 – the Lower and Middle Groups. Appl. Earth Sci. 118 (3/4), 131–161.

Okada, K., Iwashita, A., 1992. Hyper-multispectral image analysis based on waveform characteristics of spectral curve. Adv. Space Res. 12, 433–442.

Pirard, E., Bernhardt, H.J., Catalina, J.C., Brea, C., Segundo, F., Castroviejo, R., 2008. From spectrophotometry to multispectral imaging of ore minerals in visible and near infrared (VNIR) microscopy. In: Proceedings of the Ninth International Congress for Applied Mineralogy. Brisbane, Australia (8–10 September, 2008), pp. 1–6.

Proenza, J., Gervilla, F., Melgarejo, J.C., Bodinier, J.L., 1999. Al-rich and Cr-rich chromitites from the Mayarí-Baracoa ophiolitic belt (eastern Cuba): consequence of interaction between volatile-rich melts and peridotites in suprasubduction mantle. Econ. Geol. 94, 547–566.

Rawlings, J.O., Pantula, S.G., Dickey, D.A., 2001. Applied Regression Analysis: A Research Tool. Springer Science & Business Media, New York.

Williams, K.B., Jackson, C.R.M., Ceek, L.C., Donaldson, H., Parman, S.W., Pieters, C.M., Dyar, M.D., Prissel, T.C., 2016. Reflectance spectroscopy of chromium-bearing spinel with application to recent orbital data from the Moon. Am. Mineral. 101, 726–734.

Zhou, M.F., Kerrich, R., 1992. Morphology and composition of chromite in komatiites from the Belingwe Greenstone belt, Zimbabwe. Can. Mineral. 30, 303–317.